



Ag doping of Zn-In-S quantum dots for photocatalytic hydrogen evolution: Simultaneous bandgap narrowing and carrier lifetime elongation

Guan Gong¹, Yanhong Liu¹, Baodong Mao*, Lili Tan, Yalin Yang, Weidong Shi*

School of Chemistry and Chemical Engineering, Jiangsu University, Zhenjiang 212013, PR China



ARTICLE INFO

Article history:

Received 14 February 2017

Received in revised form 16 May 2017

Accepted 19 May 2017

Available online 22 May 2017

Keywords:

Photocatalysis

Hydrogen evolution

I–III–VI

Quantum dots

Time-resolved photoluminescence

ABSTRACT

Visible-light-driven photocatalytic hydrogen production has been an ongoing hot topic for clean and renewable energy, for which I–III–VI multinary metal sulfides play an important role owing to their unique ability of bandgap manipulation by composition. In this work, we present the controlled synthesis and hydrogen evolution property of a series of Ag:Zn-In-S quantum dots (QDs) in an effort to a more comprehensive understanding of Ag doping. With increasing ratio of Ag, the UV-vis absorption and photoluminescence wavelength was observed to be tuned in a wide range from light green to dark red. With increased Ag doping, dramatic increase (over 70 times) of the photocatalytic activity was observed (maximized with Ag:In:Zn ratio of 1.5:10:5). More importantly, time-resolved photoluminescence study reveals that this synergistic enhancement effect of the photocatalytic activity by controllable Ag doping was correlated with the simultaneous bandgap narrowing and carrier lifetime elongation, which contribute to the enhanced visible light absorption and charge separation, respectively. The enhanced charge separation upon Ag doping were further proved by photocurrent and electrochemical impedance spectra measurements. A mechanism is proposed for this synergistic effect of photocatalysis by suitable Ag doping, where the long-lived deep donor-acceptor pair states play an important role. Our results provide an interesting view and useful guideline for photocatalyst design using the narrow bandgap multinary sulfides.

© 2017 Elsevier B.V. All rights reserved.

1. Introduction

An enormous amount of effort has been made to pursue sustainable and efficient hydrogen production as an environmentally friendly and clean energy by utilizing inexhaustible solar energy [1–3]. Up to now, a large number of semiconductor photocatalysts have been developed for hydrogen production [4–8]. In this field, one of the most critical challenges is the development of visible-light active photocatalysts. Traditional photocatalysts including TiO₂ and other oxide semiconductors are impaired owing to their wide bandgap (>3 eV), which requires ultraviolet irradiation that only accounts for less than 4% of the solar energy [9]. It is an inevitable task to exploit the development of photocatalyst for the effective utilization of the over 40% solar energy in visible range [1].

As the first reported effective strategy for narrow bandgap photocatalyst in 2004 [8], I–III–VI chalcogenide semiconductors and derived solid solutions have attracted great attention in photocatalytic hydrogen production, because of their highly tunable compositions, unique optical properties and significant solar-harvesting abilities [10–17]. Early reports on multinary sulfide photocatalysts mainly focused on construction of solid solutions with tunable bandgaps, such as (AgIn)_xZn_{2(1-x)}S₂, ZnS–CuInS₂–AgInS₂, and ZnS–MInS₂ (M = Cu or Ag) [8,16]. Recently, more and more interest has been focused on small sized nanocrystals or quantum dots (QDs), owing to their unique quantum size effect and high surface area [18]. Kameyama et al. have studied controlling the electronic energy structure of ZnS–AgInS₂ solid solution nanocrystals for photoluminescence and photocatalytic hydrogen evolution [17]. Among the reported bandgap tuning works, the group I elements (Ag and Cu) have shown the most effective bandgap narrowing down in the I–III–VI materials [13,16]. However, it was also observed that the photocatalysts will be severely deactivated with extra Ag or Cu, which have to be controlled at a relatively low level and restrict the potential of bandgap

* Corresponding authors.

E-mail addresses: maobd@ujs.edu.cn (B. Mao), swd1978@ujs.edu.cn (W. Shi).

¹ These authors contributed equally to this work.

narrowing [11,13]. It is of great interest to elucidate the role of Ag doping and the related mechanisms for the development of visible-light photocatalytic hydrogen production.

Similar to the I–III–VI materials, ternary $ZnIn_2S_4$ has also attracted considerable interest as a rising star in visible-light photocatalysis because of its high stability and relatively high valence band energy [19–22]. Herein, we present the preparation of a series of Ag:Zn-In-S QDs by a facile hydrothermal method. Effective bandgap narrowing was observed by both of the absorption and photoluminescence (PL) spectra red shift with increasing molar ratio of Ag. The photocatalytic activities for H_2 evolution were evaluated under visible-light ($\lambda > 420$ nm) irradiation, which shows continuous increase under certain level of Ag doping ($Ag:In:Zn = 1.5:10:5$). The effect of the Ag:Zn-In-S QDs molar ratio on the photocatalytic H_2 production activity was investigated comparatively. Further PL mechanism study indicates that the intrinsic deep donor-acceptor states increase with Ag doping, which can benefit separation of the photogenerated charge carriers. Photocurrent and electrochemical impedance spectra (EIS) measurements further prove the enhanced charge separation with Ag doping. From these results, a possible mechanism for the enhanced photocatalytic activity, where a synergistic effect for photocatalysis was achieved by Ag doping through simultaneous bandgap narrowing and charge carrier lifetime elongation. Our finding provides a new understanding for the design of narrow-bandgap photocatalysts using the multinary metal sulfides.

2. Experimental

2.1. Materials

All the reagents are analytically pure and used directly without further purification. Silver nitrate ($AgNO_3$), zinc acetate ($Zn(OAc)_2 \cdot 2H_2O$), indium nitrate ($In(NO_3)_3 \cdot 4.5H_2O$), thioacetamide (TAA), sodium hydroxide (NaOH), sodium sulfite (Na_2SO_3), sodium sulfide nonahydrate ($Na_2S \cdot 9H_2O$), L-cysteine ($HSCH_2CH(NH_2)CO_2H$) and absolute ethanol were purchased from Sinopharm Chemical Reagent Co. Ltd.

2.2. Synthesis of the Ag:Zn-In-S QDs

Zn -In-S samples were prepared via a hydrothermal method according to the literature with modifications [23]. In a typical procedure, $Zn(OAc)_2 \cdot 2H_2O$ (0.85 mmol), $In(OAc)_3 \cdot 4.5H_2O$ (1.7 mmol) and excess amount of TAA (3.25 mmol) were dissolved in 35 mL of distilled water under vigorous stirring. Then, the mixed solution was transferred into a 50 mL Teflon-lined stainless steel autoclave and kept at 110 °C for 4 h, then cooled down to room temperature naturally. The synthesized sample was separated by centrifugation at 10,000 rpm and washed with ethanol/water for three times. Finally, the obtained product was redispersed in water for further use.

For the synthesis of Ag:Zn-In-S QDs, a desired amount of $AgNO_3$ solution was added into mixed solution including the zinc and indium precursors under ultrasonic treatment. Then L-cysteine aqueous solution was added under vigorous stirring. The pH value of the mixed solution was adjusted to 8.5 using 1.0 M NaOH solution. Following, excessive thioacetamide (TAA) was rapidly added to the mixture. The solution was sealed in a 50 mL Teflon-lined stainless steel autoclave and heated at 110 °C for 4 h and naturally cooled down to room temperature. The as-prepared Ag:Zn-In-S samples were collected by centrifugation and washed with water/ethanol cycles for three times. Various Ag:Zn-In-S QDs were prepared by changing the amount of the added silver stock solution into the reaction solution. The molar ratios of $Ag:In:Zn$ were

tuned systematically from 0:10:5, 0.25:10:5, 0.5:10:5, 0.75:10:5, 1:10:5, 1.5:10:5, 2:10:5, to 3:10:5. The samples were denoted as $Ag:Zn-In-S-0$ (pure Zn-In-S), $Ag:Zn-In-S-0.25$, $Ag:Zn-In-S-0.5$, $Ag:Zn-In-S-0.75$, $Ag:Zn-In-S-1$, $Ag:Zn-In-S-1.5$, $Ag:Zn-In-S-2$, and $Ag:Zn-In-S-3$, respectively.

2.3. Characterization

Structure of the samples was measured by X-ray diffraction (XRD, D8 ADVANCE, Bruker, Germany), using $Cu-K\alpha$ radiation source ($\lambda = 1.54056\text{\AA}$) at a scanning rate of 4.0°/min. Energy-dispersive X-ray spectra (EDS) were performed on an S-4800 field emission scanning electron microscope (FESEM, Hitachi, Japan). Transmission electron microscopy (TEM), high-resolution TEM (HRTEM) and scanning transmission electron microscopy (STEM) were also used to characterize the samples using a Tecnai G2 F30 S-Twin (FEI) electron microscope with an accelerating voltage of 200 kV. UV-vis absorption spectra was recorded with a Cary 8454 spectrophotometer, while the PL spectra of the samples were measured on a Cary Eclipse fluorescence spectrophotometer with an excitation wavelength of 450 nm. The PL quantum yield (QY) was measured by comparing with Rhodamine B aqueous solution as the standard. Time-resolved PL spectra were collected using a QuantaMaster™ 40 spectrometer (Photon Technology International, Inc.) excited at 481 nm. The X-ray photoelectron spectra (XPS) were obtained using a Near Ambient Pressure XPS spectrometer (SPECS Company). The photocurrent and electrochemical impedance spectra were carried out by a CHI 660B electrochemical workstation (CH Instruments, Inc., China) with a standard three-electrode cell at room temperature.

2.4. Photocatalytic hydrogen production

The photocatalytic H_2 production was carried out in a Lab- H_2 photocatalytic system. A 300 W xenon lamp with an optical filter ($\lambda > 420$ nm) was applied as the light source and vertically placed on top of the reactor. In a typical experiment, 50 mg of the as-prepared QD photocatalyst was dispersed with vigorous stirring in 100 mL of aqueous solution including 0.25 M Na_2SO_3 and 0.35 M Na_2S as the sacrificial reagents and stirred continuously to ensure uniform irradiation of the catalyst suspension during the whole experiment. A certain amount of $H_2PtCl_6 \cdot 6H_2O$ aqueous solution was dripped into the system for loading 2 wt% of Pt nanoparticles onto the photocatalyst surface by photochemical reduction deposition. Before irradiation, the system was vacuumed for 20 min to remove dissolved oxygen in the solution. During the whole reaction process, a certain amount of the generated gas in the reactor was collected per hour and analyzed with an online gas chromatograph (GC-7900, TCD detector) with argon as the carrier gas. In addition, the hydrogen evolution rate was also investigated under irradiation of different color lights by using single-wavelength filters (400, 420, 450 and 550 nm, Excelitas Technologies, USA), and the remaining hydrogen detection steps are similar to the above hydrogen evolution measurement.

3. Results and discussion

3.1. Structure and morphology

The Ag:Zn-In-S QDs were prepared via one-pot hydrothermal method from $Zn(OAc)_2$, $In(NO_3)_3$, L-cysteine and TAA with the introduction of different amounts of $AgNO_3$. XRD was first used for insights on silver incorporation in Zn-In-S. As shown in Fig. 1a, XRD patterns of the Ag:Zn-In-S QDs show characteristic peaks assigned to (008), (112), and (203) planes of hexagonal phase $ZnIn_2S_4$ (ICDD-JCPDS card No. 72-0773) [19]. With Ag doping, the XRD patterns

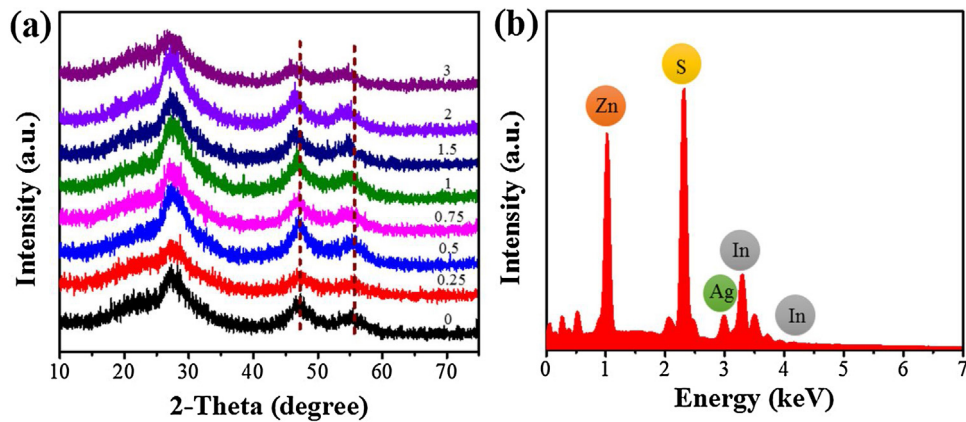


Fig. 1. (a) XRD patterns of the Ag:Zn-In-S QDs with the molar ratio of Ag:In:Zn precursors varying from 0:10:5 to 3:10:5. (b) EDS spectra of the Ag:Zn-In-S-1.5 QDs.

were almost the same as that of the pristine Zn-In-S samples, except that the diffraction peaks were slightly shifted to lower angles with increasing amount of Ag (as indicated by the dashed lines in Fig. 1a). This down shift is due to the larger ionic radius of Ag^+ (1.26 Å) compared to that of Zn^{2+} (0.74 Å) and In^{3+} (0.81 Å) [24]. This observation suggests that Ag^+ are incorporated into the lattice of Zn-In-S. In addition, we did not observe any impurity diffraction peaks like silver sulfides or oxides in the XRD patterns, indicating that silver inoculation during the synthesis process did not produce other phases. The existence of silver in the samples was further proved by EDS that showed the peaks associated with Zn, In, S and Ag, suggesting that Ag^+ are successfully incorporated into Zn-In-S, as shown in Fig. 1b.

TEM is used to study the morphology and size of the Ag:Zn-In-S samples. TEM and HRTEM images of the Ag:Zn-In-S-1.5 QDs with different magnifications are shown in Fig. 2. Spherical and uniform particles with a narrow size distribution (inset in Fig. 2a) were observed with almost no particle aggregation. This observation indicated that high quality QDs were obtained with L-cysteine as the capping ligand at suitable pH value, even with relatively high-concentration metal precursors [23]. The average size of Ag:Zn-In-S-1.5 QDs is estimated to be 3.2 ± 0.7 nm. The HRTEM images shown in Fig. 2c reveal the relatively good crystalline structure of the QDs with continuous lattice fringes through the whole particle. The interplane spacing is about 0.32 nm, corresponding to the (102) plane of ZnIn_2S_4 . The above results indicate the successful preparation of well-defined Ag:Zn-In-S QDs.

Next, XPS was used to determine the electronic states of the as-prepared Ag:Zn-In-S-1.5 QDs. In Fig. 3a, the XPS survey spectrum of the Ag:Zn-In-S-1.5 QDs shows the existence of Ag, Zn, In, and S elements. As shown in Fig. 3b, the peaks at binding energies of 373.8 and 367.8 eV are assigned to $\text{Ag } 3d_{3/2}$ and $\text{Ag } 3d_{5/2}$, respectively. The peaks at binding energies of 452.6 and 444.9 eV could be attributed to $\text{In } 3d_{3/2}$ and $\text{In } 3d_{5/2}$, respectively (Fig. 3c). The Zn 2p spectra shows two peaks at 1045 and 1021.9 eV, corresponding to the $\text{Zn } 2p_{1/2}$ and $\text{Zn } 2p_{3/2}$, respectively (Fig. 3d). The binding energy values indicate that the chemical states of Ag, In and Zn are +1, +3, and +2, respectively, with no obvious difference from the literature values [14,25]. The S 2p XPS spectrum in Fig. 3e can be deconvoluted into two main peaks at 161.8 eV, which are consistent with a valence of -2 in metal sulfides.

Optical properties of the Ag:Zn-In-S QDs were systematically characterized, as shown in Fig. 4. The UV-vis spectra in Fig. 4a show that the absorption onset shifts to long wavelengths with an increase of doped silver. The absorption onset for Zn-In-S samples starts from around 450 nm. With increased silver doping, the onset shifts toward long wavelength and reaches as high as 800 nm, with

Table 1

Summary of bandgaps, PL peaks and PL quantum yields (QYs) of the Ag:Zn-In-S QDs.

Samples	Bandgap (eV/nm)	PL emission (eV/nm)	QYs (%)
Ag:Zn-In-S-0	3.28/378	–	0
Ag:Zn-In-S-0.25	3.02/410	2.39/519	1.28
Ag:Zn-In-S-0.5	2.86/433	2.27/547	6.4
Ag:Zn-In-S-0.75	2.73/454	2.17/570	11.5
Ag:Zn-In-S-1	2.59/478	2.07/598	12.8
Ag:Zn-In-S-1.5	2.48/500	1.99/621	9.07
Ag:Zn-In-S-2	2.28/543	1.94/639	5.47
Ag:Zn-In-S-3	2.01/617	1.89/654	2.97

a significant absorbance enhancement in the visible region. The change in absorption onset may appear as a result of an interaction between the 3d-state of silver and valence band of the Zn-In-S matrix [24]. As a result, the Ag:Zn-In-S QDs show the absorption onset red shifts from 450 to 800 nm with Ag:In ratio increasing from 0:10 to 3:10, indicating an obvious bandgap narrowing correspondingly. In the insets of Fig. 4a, the bandgaps of the Ag:Zn-In-S QDs were estimated according to the Tauc plot, $(\alpha h\nu)^2 = A(h\nu - Eg)$, for direct bandgap semiconductors, in which α , h , ν , A and Eg represent the absorption coefficient, Planck constant, light frequency, a constant and bandgap energy, respectively [30–32]. After calculation, the bandgap of the Ag:Zn-In-S QDs decreases from 3.28 to 2.01 eV with increasing Ag (Ag:In from 0:10 to 3:10), as summarized in Table 1.

The Ag:Zn-In-S QDs also show systematically tunable PL by changing the ratio of the silver dopant. As shown in Fig. 4b, the as-prepared Zn-In-S QDs has almost no PL. With the increased silver doping, the PL peak shifts toward the red, ranging from 519 to 654 nm with Ag:In ratio of 0.25:10 to 3:10, as summarized in Table 1. The PL red shift is similar to the trend of absorption red shift and bandgap narrowing in Fig. 4a. It also can be seen from the photographs in Fig. 4c that the color of samples changes gradually from light green to dark red with increasing silver, demonstrating the effective tuning of the optical properties of the Ag:Zn-In-S QDs. Moreover, the PL QYs of the as-synthesized Ag:Zn-In-S QDs samples show a volcano type dependence on the Ag:In ratio, which increased first (with Ag:In < 1:10) and then started to decrease, as shown in Fig. 4d. The maximum PL QY of 12.8% in the Ag:Zn-In-S QDs was achieved with Ag:In:Zn ratio of 1:10:5. And with further increase of Ag doping, the PL QY of the samples decreases. The PL QY enhancement of the samples may arise the improved electronic structure of QDs resulted from suitable amount of silver doping [11]. It is known that PL of the multinary I–III–VI is mainly attributed to the intrinsic defect states, e.g. the deep donor–acceptor pair (DAP) states [10,30]. The observed PL QYs increase upon Ag doping may originate from increased density of

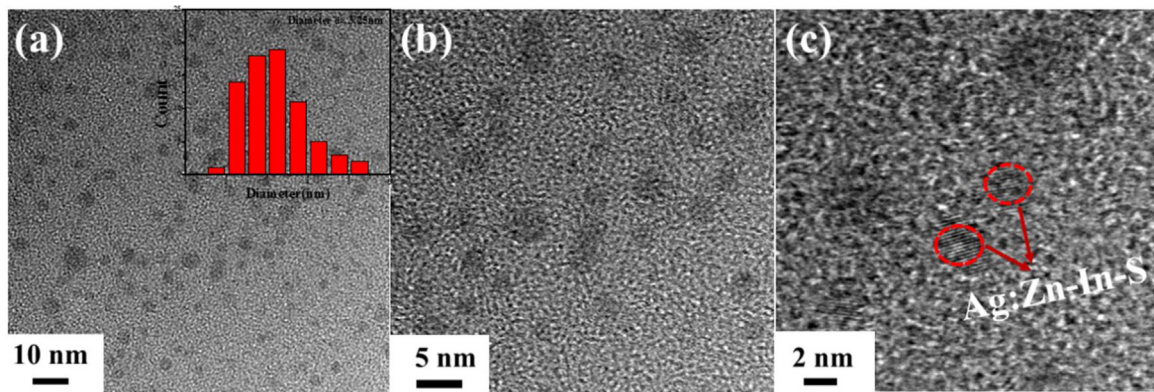


Fig. 2. TEM images of different magnifications (a and b) and HRTEM image (c) of the Ag:Zn-In-S-1.5 QDs.

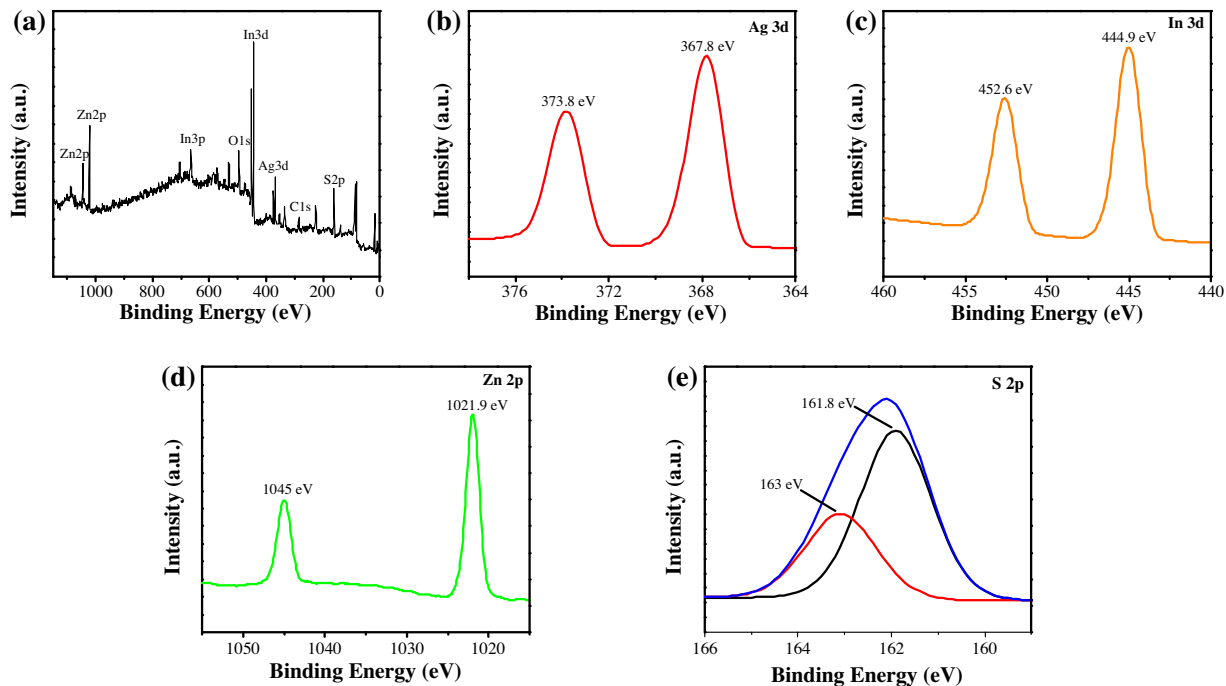


Fig. 3. XPS spectra of the Ag:Zn-In-S-1.5 QDs: (a) survey and (b–e) high-resolution spectra of Ag 3d, In 3d, Zn 2p and S 2p.

DAP states in the Ag:Zn-In-S QDs with increased incorporation of silver [12,17].

3.2. Photocatalytic hydrogen evolution

In order to study the photocatalytic activity of the Ag:Zn-In-S QDs, we performed hydrogen evolution experiments in aqueous solution of Na_2S and Na_2SO_3 under visible-light irradiation ($\lambda > 420 \text{ nm}$) with photodeposited Pt as the cocatalyst. Fig. 5(a) shows the photocatalytic activity of the Ag:Zn-In-S-1 QDs with different loading amount of Pt under visible light irradiation. H_2 production rate of $24.6 \mu\text{mol g}^{-1} \text{ h}^{-1}$ was obtained for the QDs without Pt, indicating that the Ag:Zn-In-S QDs itself is a promising candidate material for Pt-free photocatalytic water splitting [40]. The hydrogen evolution rate increased with Pt loading increasing to 0.7 wt% ($68.3 \mu\text{mol g}^{-1} \text{ h}^{-1}$) and 1 wt% ($98.0 \mu\text{mol g}^{-1} \text{ h}^{-1}$) and reached the maximum with 2 wt% of Pt ($150.1 \mu\text{mol g}^{-1} \text{ h}^{-1}$) with the $\text{Na}_2\text{SO}_3/\text{Na}_2\text{S}$ ($0.25 \text{ M}/0.35 \text{ M}$) solution under visible light irradiation. The loading of Pt on the Ag:Zn-In-S QDs greatly improved the photocatalytic efficiency because the surface loaded Pt particles can function as an efficient electron transfer promoter for H_2

production [34,35]. We observed that the photocatalytic hydrogen yield of 2 wt% Pt loaded Ag:Zn-In-S-1 QDs is 6.1 times higher than the QDs only photocatalyst without Pt. However, with further increase of Pt to 3 wt%, the hydrogen yield quickly decreased to $119.8 \mu\text{mol g}^{-1} \text{ h}^{-1}$, which may be due to the light shielding effect of the Pt cocatalyst [34,36,37]. The result suggests that 2 wt% of Pt loading works best as the efficient active site rather than shielding the incident photons, which was then employed as the standard condition in our photocatalytic system for the comparison of all the Ag:Zn-In-S QDs [8].

The time courses of photocatalytic H_2 evolution activities of the Ag:Zn-In-S QDs with different Ag content are shown in Fig. 6a. It can be seen that Zn-In-S alone exhibited poor activity ($22.6 \mu\text{mol g}^{-1}$ of hydrogen evolved in 5 h), almost negligible compared to that of the best sample (Ag:Zn-In-S-1.5 QDs, $1640.2 \mu\text{mol g}^{-1}$ in 5 h). As the Ag dopant was increased, the photocatalytic H_2 production activity of the samples was remarkably enhanced as shown in Fig. 6b, which can be attributed to the decreased bandgap and largely enhanced visible-light absorption of the Ag:Zn-In-S QDs. The Ag:Zn-In-S-1.5 QDs showed highest photocatalyst activity of H_2 production with the rate of $328.04 \mu\text{mol g}^{-1} \text{ h}^{-1}$, more than 70 times higher than

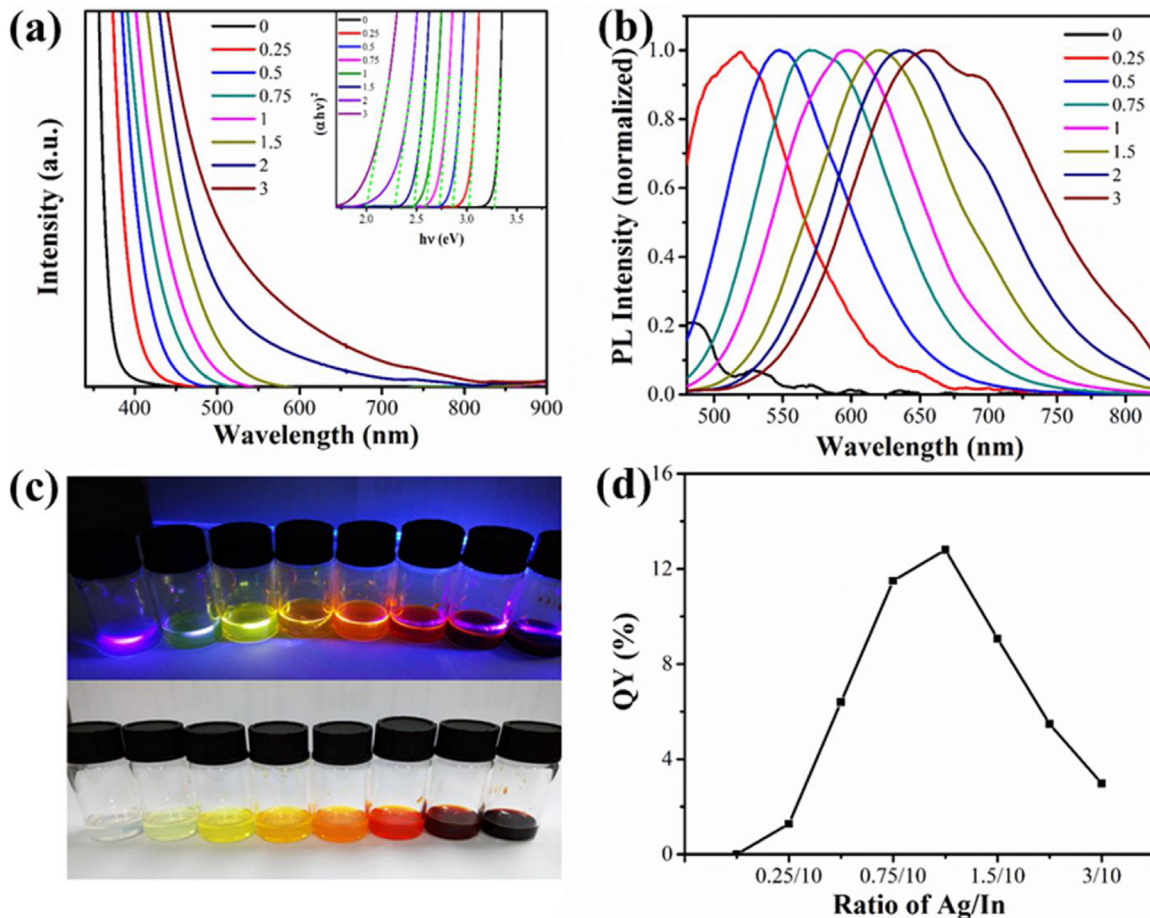


Fig. 4. (a) UV–vis absorption spectra, (b) PL spectra, (c) digital photographs under UV excitation (upper image) and room light (lower image), and (d) PL QYs of the Ag:Zn-In-S QDs with different amount of Ag.

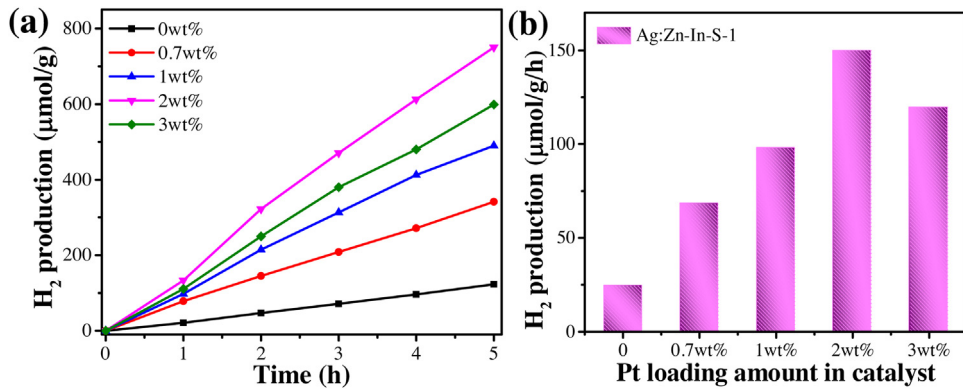


Fig. 5. (a) Time-dependent H₂ evolution of the Ag:Zn-In-S-1 QDs with different Pt content as the cocatalyst under visible light irradiation ($\lambda > 420$ nm). (b) Comparison of the H₂ evolution rate for the Ag:Zn-In-S-1 QDs.

the undoped Zn-In-S QDs ($4.52 \mu\text{mol g}^{-1} \text{h}^{-1}$). With even more Ag introduction (Ag:In:Zn above 1.5:10:5), the photocatalytic activity started to decrease, though the visible light absorption is enhanced (Fig. 4a). This phenomenon may be attributed to that the increased DAP states introduced by excessive single element doping can also act as the combination centers of the photo-generated carriers, which would reduce the catalytic rate. The electron-hole recombination center is reported to reduce the mobility of the photo-generated charge carriers [26]. Based on these results, we can see that Ag doping enhanced the photocatalytic evolution rate dramatically with Ag:In ratio as high as 1.5:10 due to the increased

visible-light absorption until too much silver is introduced. This is already a much higher doping level compared to that in I-III-VI microspheres, which may be due to the short diffusion length in the QDs.

We have performed the hydrogen evolution over the Ag:Zn-In-S-1.5 QDs with different color light by using a series of single-wavelength cutoff filters (400, 420, 450 and 550 nm). As shown in Fig. 7, the variation of the hydrogen evolution rate is in good agreement with the UV–vis absorption spectra. Hydrogen evolution stopped in the absorption tail region (>550 nm), revealing that the visible-light response of the photocatalyst is

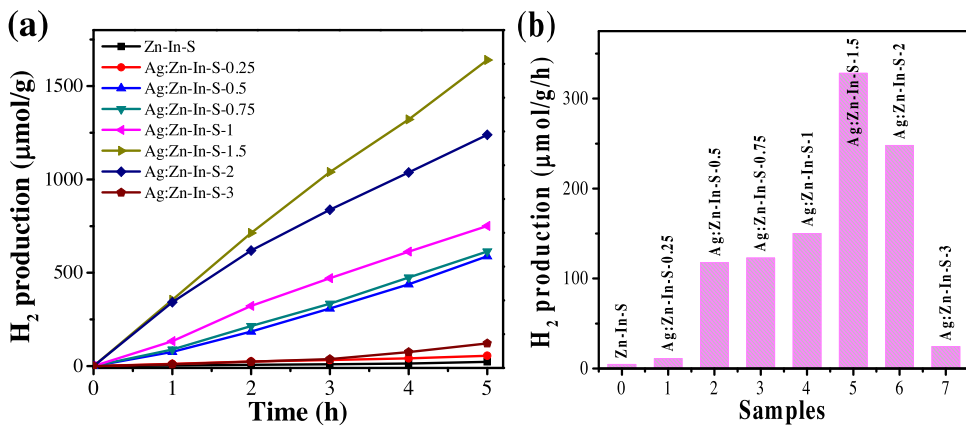


Fig. 6. (a) Time-dependent H₂ evolution of the Ag:Zn-In-S QDs with different Ag content under visible light irradiation ($\lambda > 420$ nm). (b) Comparison of the H₂ evolution rate for the Ag:Zn-In-S QDs.

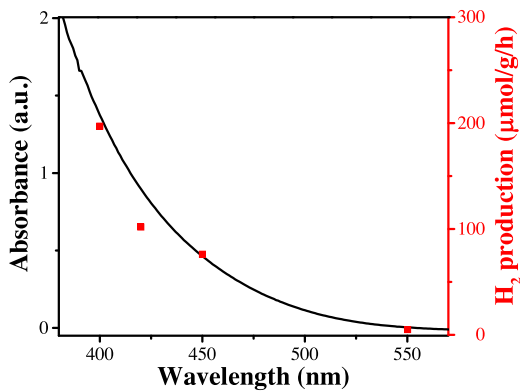


Fig. 7. UV-vis absorption curve (left) and hydrogen evolution rate (right) of the Ag:Zn-In-S-1.5 QDs with 2 wt% Pt as co-catalyst under irradiation of different color visible light.

due to the band-gap transition that was controlled by the chemical composition of the QDs. At 400 nm, the H₂ evolution rate of the Ag:Zn-In-S-1.5 QDs was as high as 196.98 μmol g⁻¹ h⁻¹. The H₂ evolution rate decreased with increasing wavelength until the lowest value of 5.04 μmol g⁻¹ h⁻¹ around 550 nm. Hydrogen evolution was not detected with further wavelength increase to 600 nm, suggesting that only photons with energy larger than ~2 eV (wavelength shorter than 600 nm) can induce the photocatalytic reaction, which agrees well with the bandgap value of 2.48 eV of the Ag:Zn-In-S-1.5 QDs.

Besides the hydrogen evolution rate, morphology and elemental mapping of the Pt loaded Ag:Zn-In-S QDs were further investigated by HRTEM and HAADF-STEM (Fig. 8). As shown in Fig. 8a, the QDs show uniform size distribution and almost no particle aggregation after Pt loading under visible light irradiation for 2 h. Fig. 8(b) shows clear lattice fringes with d-spacing of 0.22 nm and 0.32 nm, corresponding to the (111) plane of Pt and (102) plane of ZnIn₂S₄, respectively, indicating that the two phases were successfully combined together. To further clarify the beneficial effect of Pt, we performed elemental mapping of the Pt loaded QDs, which reveals that the Ag, In, Zn, S and Pt elements coexist and distribute uniformly in the QDs (Fig. 8c). The relatively weaker intensity and uniform distribution of Pt are good evidence for the immobilized Pt nanoparticles on the QDs [14].

The stability of the catalyst is another important parameter for the photocatalytic performance in practical applications. Fig. 9 shows the photocatalytic activity of the Ag:Zn-In-S-1.5 QDs decreased slightly after three runs of reaction under visible

Table 2
PL decay parameters of the Ag:Zn-In-S QDs.

Samples	A ₁ /%	τ ₁ /ns	A ₂ /%	τ ₂ /ns	τ _{ave} /ns
Ag:Zn-In-S-0.5	66.74	2.50	33.24	195.94	66.79
Ag:Zn-In-S-1	15.84	12.58	84.16	316.91	268.70
Ag:Zn-In-S-1.5	0	–	100	293.73	293.73

light irradiation ($\lambda > 420$ nm). The initial photocatalytic H₂ yield was 1640.2 μmol g⁻¹ in the first 5 h (328.04 μmol g⁻¹ h⁻¹). After three reaction runs, the photocatalyst retains 91.7% of the initial activity and reached a hydrogen yield of 1504.5 μmol g⁻¹ in 5 h (300.9 μmol g⁻¹ h⁻¹). The slightly decreased hydrogen evolution rate may be attributed to the increased concentration of the oxidation state of sacrificial reagents and the aggregation of the QDs [33,34,38,39]. It reveals that the sample possesses relatively good stability under the SO₃²⁻/S²⁻ solution as sacrificial reagents for its practical application. Meanwhile, the XRD of Ag:Zn-In-S-1.5 QDs after 15 h photoreaction was characterized, shown in Fig. 9b. The XRD patterns indicate that the phase and structure of the samples show no obvious change. It further proves that the Ag:Zn-In-S QDs are stable.

3.3. Mechanism study of the photocatalytic activity enhancement

To further explore the mechanism of photocatalytic activity variation of the Ag:Zn-In-S QDs upon Ag incorporation, time-resolved PL spectra were performed under an excitation of 481 nm laser. It is reported that the PL lifetime could reflect the recombination and transfer of the photogenerated charge carriers [10]. As shown in Fig. 10, the PL decay curves (dotted curves in Fig. 10) of the QDs were fitted using a biexponential function $I(t) = A_1 * \exp(-t/\tau_1) + A_2 * \exp(-t/\tau_2)$ and the average lifetime is estimated by $\tau_{ave} = (A_1\tau_1 + A_2\tau_2)/(A_1 + A_2)$, where $I(t)$ is the PL intensity at a certain delay time, A_1 and A_2 represent the relative weights of the decay components at $t=0$, and τ_1 and τ_2 are the lifetimes corresponding to different recombination pathways. Table 2 shows the PL lifetime of samples with different Ag:In ratios. With increasing Ag content, the PL lifetime of the Ag:Zn-In-S QDs increases rapidly ($\tau_{ave} = 66.79, 268.70$ and 293.73 ns corresponding the Ag:In:Zn ratios of 0.5–1.5:10:5), indicating the increased lifetime of the photogenerated electrons and holes that will benefit the charge separation and diffusion for photocatalysis. Moreover, the long-lifetime component becomes more and more important, as showing increased A_2 from 33% to 84% and 100% for Ag: In from 0.5:10 to 1:10 and 1.5:10, respectively. According to previous reports, the shorter lifetime can be attributed to surface

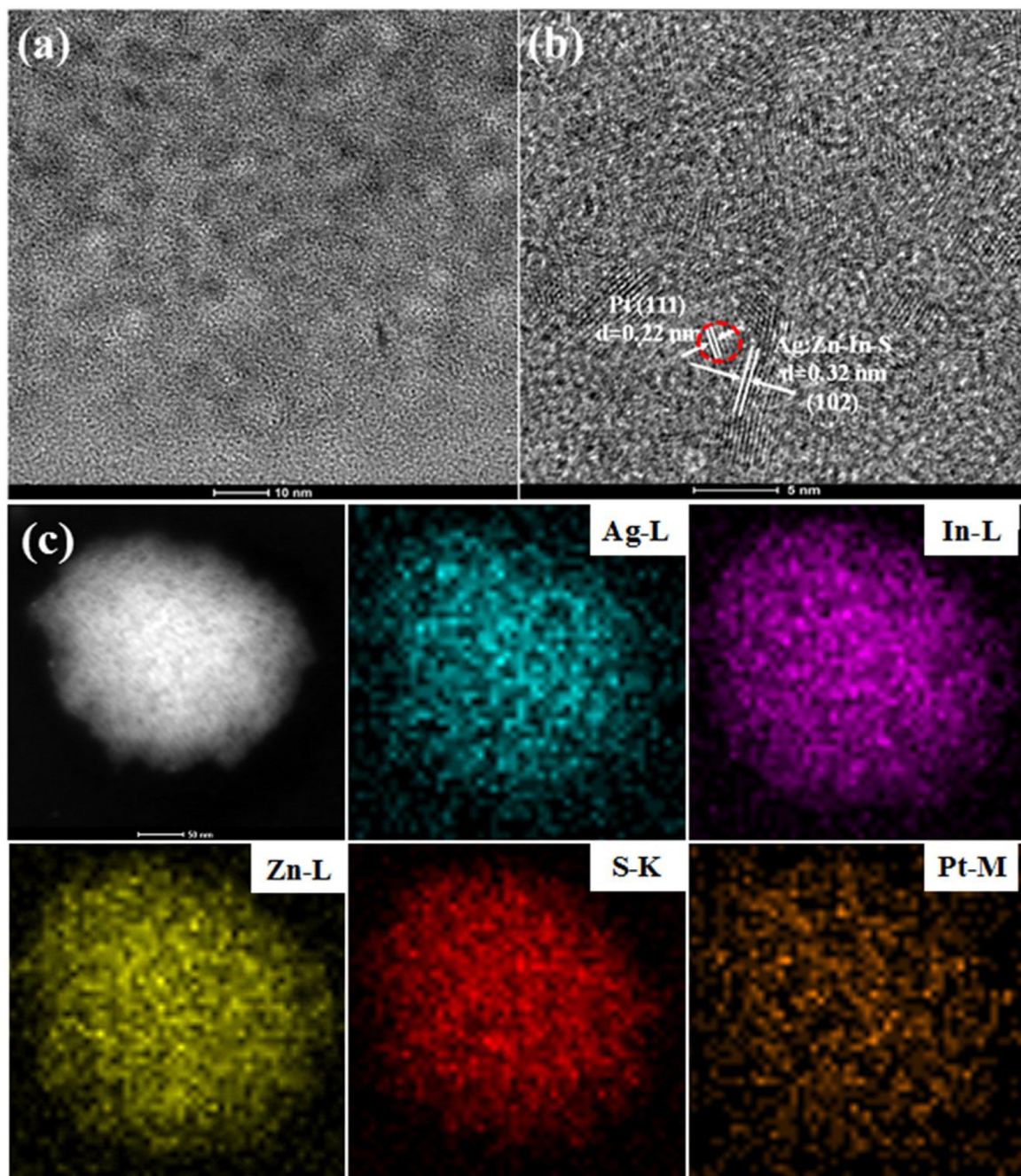


Fig. 8. (a) TEM and (b) HRTEM images of Ag:Zn-In-S QDs after 2 wt% Pt loading under visible light irradiation for 2 h. (c) HAADF-STEM image and the spatially resolved Ag, In, Zn, S and Pt elements of the Pt-2 wt% Ag:Zn-In-S QDs.

trap states, the longer lifetime could be ascribed to intrinsic deep donor-acceptor states in the mutinary I–III–VI QDs [27–29]. This observation indicates that the ratio of deep donor-acceptor states vs. surface defect states is effectively increased with silver doping, giving elongated lifetime of the photogenerated charge carriers. This result together with the observed bandgap narrowing (Fig. 4a), resulted in the increased light absorption and charge separation, which contributed synergistically to the enhancement of photocatalytic activity.

In order to further investigate the separation of photogenerated charge carries in the photocatalysts, photocurrents of the Zn-In-S and Ag:Zn-In-S QDs samples deposited on FTO glasses were performed in an on-and-off cycle mode under visible-light irradiation with an applied bias of 0.5 V. As shown in Fig. 11a, the Ag:Zn-

In-S-1.5 QDs with the highest H₂ evolution rate shows higher photocurrent value than the other two samples, which can be ascribed to the increased charge separation by deep donor-acceptor states from excess Ag-doping [24], where the photogenerated electrons and holes separate efficiently, giving prolonged lifetime of electrons and holes and improved photocatalytic activity. Electrochemical impedance spectroscopy (EIS) is also an effective way for exploring the charge-separation processes in the semiconductor-electrolyte interface. The Nyquist plots of the samples are displayed in Fig. 11b. It can be seen that the Ag:Zn-In-S-1.5 QDs exhibits a circular radius smaller than other samples. As known, the electron lifetime reflects the resistance of recombination, whereas the larger semicircle radius of EIS implies larger electron/hole recombination resistance [11]. This result suggests that a decrease of the charge

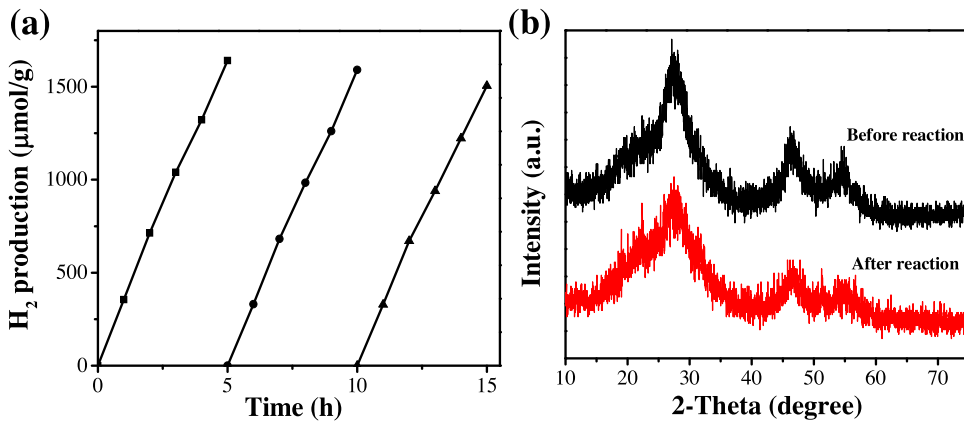


Fig. 9. (a) Stability study of photocatalytic H_2 evolution by Ag:Zn-In-S-1.5 QDs under visible light irradiation ($\lambda > 420$ nm). (b) The XRD patterns of Ag:Zn-In-S-1.5 QDs as-prepared and after three cycle runs of photocatalytic experiments.

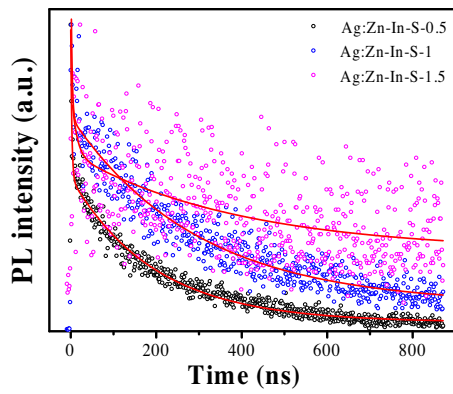
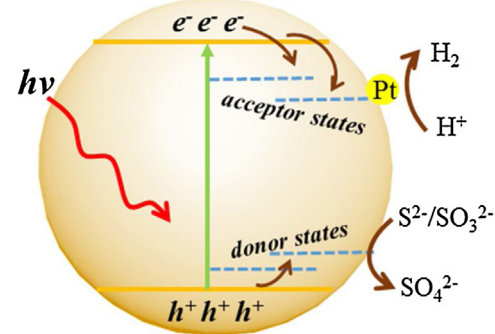


Fig. 10. PL decay curves (dots) and the corresponding biexponential fittings (solid lines) of the Ag:Zn-In-S QDs with increased introduction of silver.

transfer resistance is achieved and the electron/hole recombination in Ag:Zn-In-S-1.5 QDs is suppressed compared to other samples. With further increase of Ag doping (Ag:Zn-In-S-2), the semicircle radius of EIS shows slightly increase, indicating the larger recombination rates [11]. Therefore, the result further demonstrates that constructing of Ag-doped Zn-In-S QDs can improve the preferable efficiency of charge separation and transfer as long as the dopant concentration is controlled in a certain range.

Based on the above results and discussions, a plausible mechanism is proposed for the photocatalytic H_2 evolution of the Ag:Zn-In-S QDs, as shown in Fig. 12. The enhancement of photocatalytic activity by Ag doping are mainly attributed to the synergistic



Ag:Zn-In-S QDs

Fig. 12. Schematic illustration of the mechanism for the enhanced charge separation and photocatalytic activity in the Ag:Zn-In-S QDs.

effect of two factors: the increased light absorption and charge separation. Ag doping first resulted in the bandgap narrowing down and enhanced visible light absorption. More importantly, increased Ag incorporation in the Ag:Zn-In-S QDs resulted in the elongation of carrier lifetime due to increase of the long-lived deep donor-acceptor states. The enhanced charge separation was also proved by photocurrent and EIS. The introduction of Ag results in the formation of more deep donor-acceptor states and subsequently facilitates the effective separation of photogenerated electrons and holes, and the charge transfer to the surface catalytic sites (the Pt co-catalyst here). Yu et al. also reported that $\text{CuIn}_{1-x}\text{Ga}_x\text{S}_2$ nanocrystals

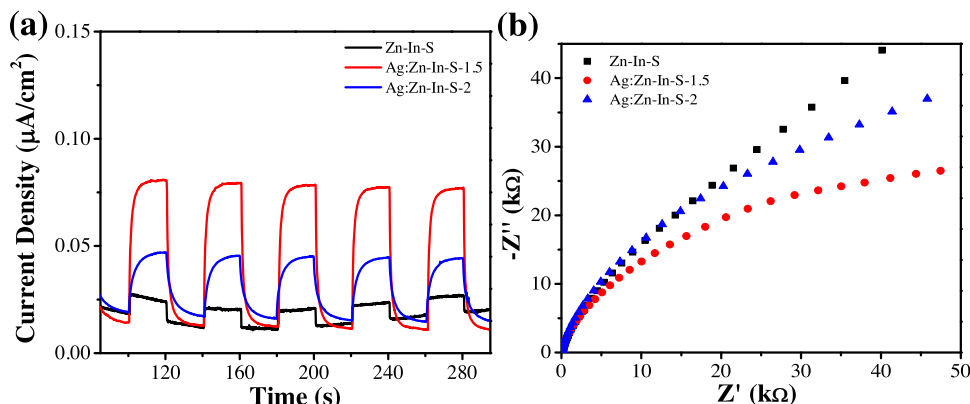


Fig. 11. (a) The transient photocurrent responses and (b) electrochemical impedance spectroscopy plots of the Zn-In-S and Ag:Zn-In-S QDs.

with increasing Ga content provides a larger driving force for charge transfer [33]. However, the long-lived trap states introduced by excessive single element doping often can act as recombination centers of photogenerated charge carriers, which would reduce the catalytic rate. Herein, the optimum compromise between the bandgap narrowing, charge separation and recombination was reached with Ag:Zn-In-S-1.5.

4. Conclusions

In summary, series of Ag:Zn-In-S QDs with different amount of Ag were synthesized by a facile hydrothermal method. Both the absorption and PL spectra shows significant red shift with increasing Ag, indicating the decreased bandgap and increased visible light utilization. Photocatalytic hydrogen evolution activity shows volcano type dependence on the concentration of Ag. More importantly, with increased Ag incorporation controlled in a suitable range (Ag:In < 1.5:10), a synergetic enhancement effect for photocatalysis was achieved with simultaneous bandgap narrowing and charge carrier lifetime increase, which may be attributed to the increased deep donor-acceptor states. Photocurrent and electrochemical impedance spectra analyses indicates the increased charge separation with Ag doping. A plausible mechanism was proposed for the role of Ag doping and the synergistic photocatalytic activity enhancement as a consequence of charge carrier separation along with bandgap decrease. Our finding provides an interesting insight and design guideline for the development of quaternary metal sulfides for visible-light-driven H₂ production.

Acknowledgments

The authors acknowledge the supports from the National Natural Science Foundation of China (21501072 and 21522603), the Jiangsu Specially-Appointed Professors Program, the Natural Science Foundation of Jiangsu Province (BK20150489), the Chinese-German Cooperation Research Project (GZ1091), the “Innovative and Entrepreneurial Doctor” Program of Jiangsu Province, the China Postdoctoral Science Foundation (2016M590419), the Jiangsu Province Postdoctoral Foundation (1501027A), and the Start Funding of Jiangsu University (15JDG011 and 15JDG027).

References

- [1] X.B. Chen, S.H. Shen, L.J. Guo, S.S. Mao, Chem. Rev. 110 (2010) 6503–6570.
- [2] T. Hisatomi, J. Kubota, K. Domen, Chem. Soc. Rev. 43 (2014) 7520–7535.
- [3] J.R. Ran, J. Zhang, J.G. Yu, M. Jaroniec, S.Z. Qiao, Chem. Soc. Rev. 43 (2014) 7787–7812.
- [4] K.F. Wu, T.Q. Lian, Chem. Soc. Rev. 45 (2016) 3781–3810.
- [5] H. Tong, S. Ouyang, Y. Bi, N. Umezawa, M. Oshikiri, J. Ye, Adv. Mater. 24 (2012) 229–251.

- [6] K. Zhang, L.J. Guo, Catal. Sci. Technol. 3 (2013) 1672–1690.
- [7] R.I. Pinhassi, D. Kallmann, G. Saper, H. Dotan, A. Linkov, A. Kay, V. Liveanu, G. Schuster, N.A. Rothschild, Nat. Commun. 7 (2016) 12552.
- [8] I. Tsuji, H. Kato, H. Kobayashi, A. Kudo, J. Am. Chem. Soc. 126 (2004) 13406–13413.
- [9] D. Cho, K.C. Ko, O.L. Garcia, S.T. Bromley, J.Y. Lee, F. Illas, J. Chem. Theory Comput. 12 (2016) 3751–3763.
- [10] J.L.Q. Song, T.T. Jiang, T.Y. Guo, L. Liu, H.J. Wang, T.Y. Xia, W.T. Zhang, X.C. Ye, M.Y. Yang, L.X. Zhu, R.X. Xia, X.L. Xu, Inorg. Chem. 54 (2015) 1627–1633.
- [11] T. Torimoto, T. Kameyama, S. Kuwabata, J. Phys. Chem. Lett. 5 (2014) 336–347.
- [12] S.L. Shen, Q.B. Wang, Chem. Mater. 25 (2013) 1166–1178.
- [13] M.D. Regulacio, M.-Y. Han, Acc. Chem. Res. 49 (2016) 511–519.
- [14] K. Li, B. Choi, T.Y. Peng, J. Mao, L. Zan, ACS Catal. 3 (2013) 170–177.
- [15] Z.F. Liu, K.Y. Guo, J.H. Han, Y.J. Li, T. Cui, B. Wang, J. Ya, C.L. Zhou, Small 10 (2014) 3153–3161.
- [16] I. Tsuji, H. Kato, A. Kudo, Angew. Chem. Int. Ed. 44 (2005) 3565–3568.
- [17] T. Kameyama, T. Takahashi, T. Machida, Y. Kamiya, T. Yamamoto, S. Kuwabata, T. Torimoto, J. Phys. Chem. C 119 (2015) 24740–24749.
- [18] W.J. Zhang, D.Z. Li, M. Sun, Y. Shao, Z.X. Chen, G.C. Xiao, X.Z. Fu, J. Solid State Chem. 183 (2010) 2466–2474.
- [19] W.L. Yang, L. Zhang, J.F. Xie, X.D. Zhang, Q.H. Liu, T. Yao, S.Q. Wei, Q. Zhang, Y. Xie, Angew. Chem. Int. Ed. 55 (2016) 6716–6720.
- [20] G.H. Tian, Y.J. Chen, Z.Y. Ren, C.G. Tian, K. Pan, W. Zhou, J.Q. Wang, H.G. Fu, Chem. Asian J. 5 (2014) 1291–1297.
- [21] Y.J. Yuan, J.R. Tu, Z.J. Ye, D.Q. Chen, B. Hu, Y.W. Huang, T.T. Chen, D.P. Cao, Z.T. Yu, Z.G. Zou, Appl. Catal. B Environ. 188 (2016) 13–22.
- [22] W. Chen, T.Y. Liu, T. Huang, X.H. Liu, X.J. Yang, Nanoscale 8 (2016) 3711–3719.
- [23] Y.J. Chen, R.K. Huang, D.Q. Chen, Y.S. Wang, W.J. Liu, X.N. Li, Z.H. Li, ACS Appl. Mater. Interfaces 4 (2012) 2273–2279.
- [24] S.H. Shen, L. Zhao, Z.H. Zhou, L.J. Guo, J. Phys. Chem. C 112 (2008) 16148–16155.
- [25] J.L.Q. Song, T.T. Jiang, G.W. Ji, W.T. Zhang, X.Y. Cheng, W. Weng, L.X. Zhu, X.L. Xu, RSC Adv. 5 (2015) 95943–95952.
- [26] Y.Z. Hong, C.S. Li, G.Y. Zhang, Y.D. Meng, B.X. Yin, Y. Zhao, W.D. Shi, Chem. Eng. J. 299 (2016) 74–84.
- [27] B.D. Mao, C.H. Chuang, C. McCleese, J.J. Zhu, C. Burda, J. Phys. Chem. C 118 (2014) 13883–13889.
- [28] Y.H. Liang, S.L. Lin, L. Liu, J.S. Hu, W.Q. Cui, Appl. Catal. B Environ. 164 (2015) 192–203.
- [29] Q.H. Zhang, Y. Tian, C.F. Wang, S. Chen, RSC Adv. 6 (2016) 47616–47622.
- [30] B.D. Mao, C.H. Chuang, J.W. Wang, C. Burda, J. Phys. Chem. C 115 (2011) 8945–8954.
- [31] A. Guchhait, A.J. Pal, ACS Appl. Mater. Interfaces 5 (2013) 4181–4189.
- [32] F. Ozel, E. Aslan, B. Istanbullu, O. Akay, I.H. Patir, Appl. Catal. B Environ. 5 (2016) 67–73.
- [33] X.L. Yu, X.Q. An, A. Shavel, M. Ibanez, A. Cabot, J. Mater. Chem. A 2 (2014) 12317–12322.
- [34] N.Z. Bao, L.M. Shen, T. Takata, K. Domen, Chem. Mater. 20 (2008) 110–117.
- [35] J. Zhang, J.G. Yu, M. Jaroniec, J.R. Gong, Nano Lett. 12 (2012) 4584–4589.
- [36] Y.B. Wang, Y.S. Wang, R. Xu, J. Phys. Chem. C 117 (2013) 783–790.
- [37] L. Zhang, X.L. Fu, S.G. Meng, X.L. Jiang, J.H. Wang, S.F. Chen, J. Mater. Chem. A 3 (2015) 23732–23742.
- [38] J.H. Yang, H.J. Yan, X.L. Wang, F.Y. Wen, Z.J. Wang, D.Y. Fan, J.Y. Shi, C. Li, J. Catal. 290 (2012) 151–157.
- [39] Y.X. Li, G. Chen, Q. Wang, A. Zhou, Z.Y. Shen, Adv. Funct. Mater. 20 (2010) 3390–3398.
- [40] X.Y. Liu, H. Chen, R.L. Wang, Y.Q. Shang, Q. Zhang, W. Li, G.Z. Zhang, J. Su, C.T. Dinh, F.P.G. de Arquer, J. Li, J. Jiang, Q.X. Mi, R. Si, X.P. Li, Y.H. Sun, Y.T. Long, H. Tian, E.H. Sargent, Z.J. Ning, Adv. Mater. (2017) 1605646.